

NASA/TM—2000-210377



# Optical Measurement and Visualization in High-Pressure, High-Temperature, Aviation Gas Turbine Combustors

Yolanda R. Hicks  
Glenn Research Center, Cleveland, Ohio

Randy J. Locke  
Dynacs Engineering Company, Inc., Brook Park, Ohio

Robert C. Anderson  
Glenn Research Center, Cleveland, Ohio

## The NASA STI Program Office . . . in Profile

Since its founding, NASA has been dedicated to the advancement of aeronautics and space science. The NASA Scientific and Technical Information (STI) Program Office plays a key part in helping NASA maintain this important role.

The NASA STI Program Office is operated by Langley Research Center, the Lead Center for NASA's scientific and technical information. The NASA STI Program Office provides access to the NASA STI Database, the largest collection of aeronautical and space science STI in the world. The Program Office is also NASA's institutional mechanism for disseminating the results of its research and development activities. These results are published by NASA in the NASA STI Report Series, which includes the following report types:

- **TECHNICAL PUBLICATION.** Reports of completed research or a major significant phase of research that present the results of NASA programs and include extensive data or theoretical analysis. Includes compilations of significant scientific and technical data and information deemed to be of continuing reference value. NASA's counterpart of peer-reviewed formal professional papers but has less stringent limitations on manuscript length and extent of graphic presentations.
- **TECHNICAL MEMORANDUM.** Scientific and technical findings that are preliminary or of specialized interest, e.g., quick release reports, working papers, and bibliographies that contain minimal annotation. Does not contain extensive analysis.
- **CONTRACTOR REPORT.** Scientific and technical findings by NASA-sponsored contractors and grantees.

- **CONFERENCE PUBLICATION.** Collected papers from scientific and technical conferences, symposia, seminars, or other meetings sponsored or cosponsored by NASA.
- **SPECIAL PUBLICATION.** Scientific, technical, or historical information from NASA programs, projects, and missions, often concerned with subjects having substantial public interest.
- **TECHNICAL TRANSLATION.** English-language translations of foreign scientific and technical material pertinent to NASA's mission.

Specialized services that complement the STI Program Office's diverse offerings include creating custom thesauri, building customized data bases, organizing and publishing research results . . . even providing videos.

For more information about the NASA STI Program Office, see the following:

- Access the NASA STI Program Home Page at <http://www.sti.nasa.gov>
- E-mail your question via the Internet to [help@sti.nasa.gov](mailto:help@sti.nasa.gov)
- Fax your question to the NASA Access Help Desk at (301) 621-0134
- Telephone the NASA Access Help Desk at (301) 621-0390
- Write to:  
NASA Access Help Desk  
NASA Center for Aerospace Information  
7121 Standard Drive  
Hanover, MD 21076

NASA/TM—2000-210377



# Optical Measurement and Visualization in High-Pressure, High-Temperature, Aviation Gas Turbine Combustors

Yolanda R. Hicks  
Glenn Research Center, Cleveland, Ohio

Randy J. Locke  
Dynacs Engineering Company, Inc., Brook Park, Ohio

Robert C. Anderson  
Glenn Research Center, Cleveland, Ohio

Prepared for the  
EOS/SPIE Symposium on Applied Photonics  
cosponsored by the European Optical Society and  
the International Society for Optical Engineering  
Glasgow, Scotland, May 22–25, 2000

National Aeronautics and  
Space Administration

Glenn Research Center

## Acknowledgments

The authors are grateful for the support of the technicians and operations engineers, without whose efforts these tests could not occur. The authors also gratefully acknowledge the technical advice of Drs. C. Wey, Y. Gu, E. Rothe, and M. Foust.

This report contains preliminary findings, subject to revision as analysis proceeds.

Trade names or manufacturers' names are used in this report for identification only. This usage does not constitute an official endorsement, either expressed or implied, by the National Aeronautics and Space Administration.

Available from

NASA Center for Aerospace Information  
7121 Standard Drive  
Hanover, MD 21076  
Price Code: A03

National Technical Information Service  
5285 Port Royal Road  
Springfield, VA 22100  
Price Code: A03

Available electronically at <http://gltrs.grc.nasa.gov/GLTRS>

# Optical measurement and visualization in high-pressure, high-temperature, aviation gas turbine combustors

Yolanda R. Hicks and Robert C. Anderson  
National Aeronautics and Space Administration  
Glenn Research Center  
Cleveland Ohio, 44135

Randy J. Locke  
Dynacs Engineering Company, Inc.  
Brook Park Ohio, 44142

## ABSTRACT

Planar laser-induced fluorescence (PLIF), planar Mie scattering (PMie), and linear (1-D) spontaneous Raman scattering are applied to flame tube and sector combustors that burn Jet-A fuel at a range of inlet temperatures and pressures that simulate conditions expected in future high-performance civilian gas turbine engines. Chemiluminescence arising from  $C_2$  in the flame was also imaged. Flame spectral emissions measurements were obtained using a scanning spectrometer. Several different advanced concept fuel injectors were examined. First-ever PLIF and chemiluminescence data are presented from the 60-atm gas turbine combustor facility.

## 1. INTRODUCTION

Regulations that further restrict the amount of pollutants that aircraft engines are allowed to release are imminent. In order to design efficient and environmentally friendly aviation gas turbine combustors that meet these regulations, a better understanding of the complex processes that take place within them must be developed. Optical and laser-based visualization techniques are important non-intrusive tools for visualizing flow processes, especially fuel injection and fuel/air mixing and burning within combustion chambers. It is widely recognized that the fuel-air mixing process is a critical factor in improving combustion efficiency and in minimizing pollutants such as  $NO_x$ . However, very few optical probes have been applied in realistic aviation gas turbine combustors due to additional safety issues involved in operating such continuous-flow high-pressure facilities, especially those with windows. These experiments also present additional spectroscopic challenges in dealing with complex multicomponent fuels that include polycyclic aromatic hydrocarbons (PAH) such as Jet-A<sup>1-3</sup>. In addition, one often must compromise real engine geometry to gain reasonable optical access, and the consequences of this may create unacceptable changes to the flow field or limit the operating regime of the model combustor. Since combustor designers and manufacturers desire information at actual design conditions, the design of facilities having optical access becomes somewhat problematic.

This paper describes the optically-accessible gas turbine combustor facilities at NASA Glenn Research Center (GRC) and presents examples of the implementation of optical techniques employed to visualize flow structure, fuel spray patternation, liquid fuel penetration, and combustion species. The tests were conducted using actual fuel injectors (and sometimes diffuser hardware) that are being considered for the next generation of low emissions combustors. The methods described at present are qualitative or semi-quantitative. These techniques are planar laser-induced fluorescence (PLIF) of fuel and OH, planar Mie scattering (PMie) of liquid fuel, 1-D UV Raman scattering to determine major combustion species, chemiluminescent imaging, and spectroscopy of species such as OH,  $C_2$  and CH.

PLIF has been well established in industrial systems<sup>4-8</sup>. Mie scattering is used to visualize the liquid fuel and may be combined with fuel PLIF in a variety of ways to image drop size<sup>3</sup> or describe the extent of vaporization<sup>9</sup>. Spontaneous Raman scattering has the major advantage that several species are measured simultaneously with good precision because the ratios of line intensities is independent of variations in laser intensity. Chemiluminescence of combustion intermediates has been used to study flame dynamics and to determine local equivalence ratios in spray flames<sup>10,11</sup>.

## 2. FACILITIES

### 2.1 CE5 test facility

The CE5 combustor subcomponent test facility at GRC has two test legs. Each test leg may be equipped with optically accessible combustion shells. The flame tube test leg can accommodate test hardware that will fit within the 7.62-cm x 7.62-cm flow path. This test stand is used to characterize fuel injector performance. The “sector” test leg can support flow path cross sections as large as 21.6-cm by 21.6-cm. This stand typically is used for large fuel injectors or to test the effects of arrays of injectors, or combustor sectors. Because its cross section is typically rectangular, an injector array in this facility is not a true “pie slice” from an annular combustor that matches actual geometry; rather, it is an idealized sector. The flame tube can support from 0.23 kg/s – 1.36 kg/s of inlet air and pressures up to 20-atm. The sector can flow from 0.23 kg/s – 4.1 kg/s and up to 18-atm pressure. Both rigs supply non-vitiated, preheated air from 450 K to 866 K.

The shells of each test rig are water-cooled stainless steel. The combustor liners are made from an aluminum oxide castable material, typically Greencast 94+. Up to four water-cooled window assemblies can be placed—one on each side—at the same axial location. The windows are made of 1.27-cm thick, UV-grade synthetic fused silica and have a clear aperture of 3.8-cm x 5.1-cm. These windows fit in either test leg of the CE5 test facility. The opposing distance between windows in the flame tube is 7.62 cm. For the sector, this opposing distance is 21.6 cm, although the actual flowpath may be smaller.

Figure 1 shows a schematic drawing of the flame tube housing and the window arrangement. The windows are symmetrically arranged around the circumference of the shell. The arrangement of windows in the sector shell is similar in that the windows are placed 90° apart, but the side windows are offset above the centerline by 2.54 cm, as shown in figure 2. The top and bottom windows are centered on their respective sides. For the cases described herein, three windows are employed; the fourth window station is equipped with a spark igniter, used to light the flame.

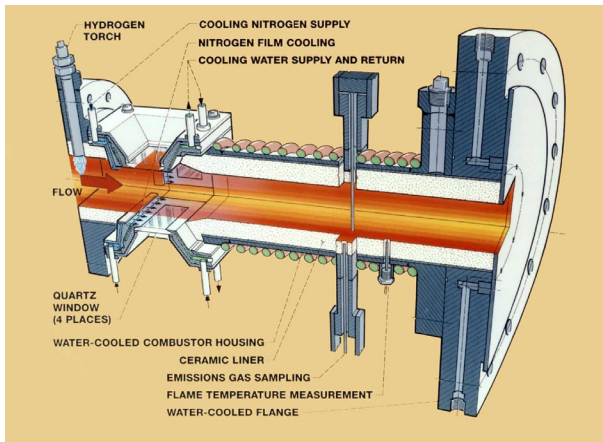


Figure 1. Schematic drawing of the CE5 flame tube.



Figure 2. Downstream-looking view within the CE5 sector combustion shell showing the arrangement of the windows and the gas sample probes.

### 2.2 ASCR facility

The third test stand can support true sectors and small annular combustors without compromising any of the actual engine geometry. This sector rig is one of two test legs in the advanced subsonic combustor rig, (ASCR, shown in figure 3). The facility can support up to 17.3 kg/s of air, preheat inlet temperatures from 395K to 980K, exhaust temperatures to 2145K, and pressures from 4 atm to 60 atm. The test stand uses a shell-in-shell approach, in which the outer shell handles the pressure stresses. The inner vessel is the sector or annular combustor with combustor liner and cooling, responsible for directing the flow and handling the stresses caused by the high combustion temperatures. The inner vessel can measure up to 0.76-m diameter by 1.2 m long. For this type of system, two sets of optical windows are needed, one for each vessel. A cartoon of the pressure vessel is shown in figure 4. The ultraviolet-grade, fused silica windows are 6.4-cm thick and have a clear aperture with diameter of 15.2 cm. Up to six window ports are circumferentially located at a single axial position along the housing: 0° (top), 60°, 90°, 180°, 270°, and 315°. Their inner surfaces lie along a circle with diameter 1.1 m. The inner shell bolts onto the downstream edge of the plenum section, just ahead of the instrumentation section, shown in red. Its windows are sized dependent on the hardware and the area of interest.

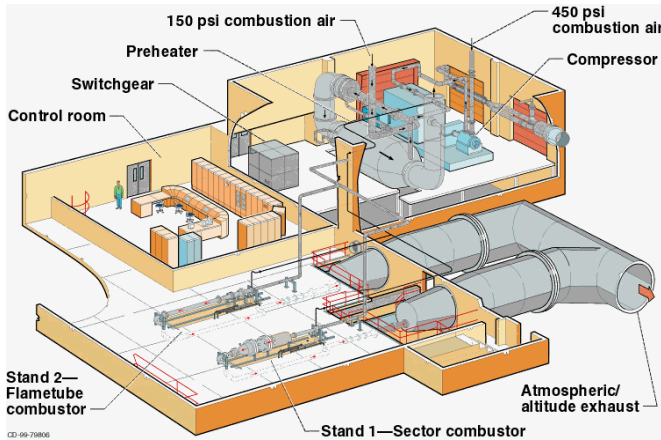


Figure 3 Schematic drawing of the advanced subsonic combustion rig (ASCR) test facility.

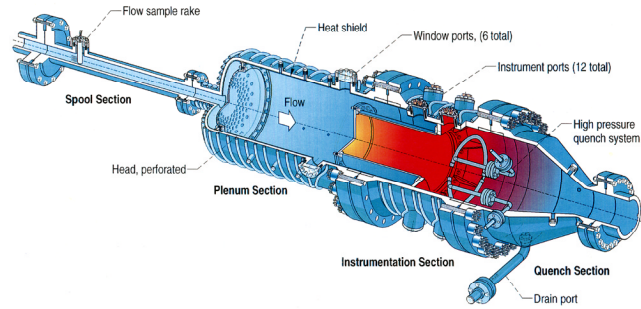


Figure 4 Drawing of the ASCR sector combustor pressure shell. Flow passes from left to right. The inner vessel that contains the actual combustor hardware bolts onto the instrumentation section.

### 2.3 Laser facilities

Each test cell has a laser room containing two pulsed laser systems, such as those depicted in the drawing of figure 5, which shows the lasers and the path taken to reach the test stands in CE5. As shown, the lasers are not physically located in the actual test cell because the cell is inaccessible during test runs for reasons of safety. Instead the laser beam(s) is transported to the test site by a series of wavelength specific remotely controlled mirrors; some mirrors are additionally mounted on traversing stages for fine positioning of the beam into the test rig. A similar scheme is used in the ASCR facility, with the main difference being that the lasers are located in a room beneath the control room pictured in figure 3. The beams are piped up through the control room ceiling and over to the sector test stand.

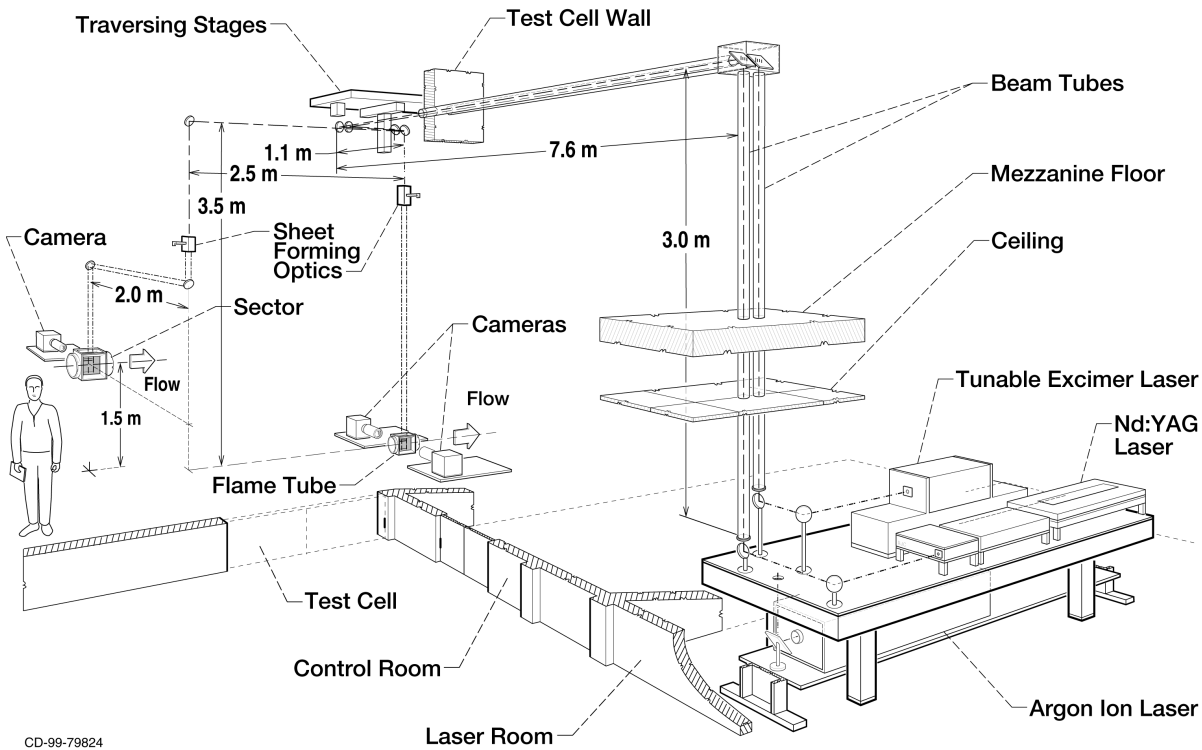


Figure 5 Laser beam path to CE5 sector and flame tube test stands.

### 3.0 EXPERIMENTAL SETUP AND METHODOLOGY

Typically, the lasers used in both test cells are 10 Hz, Nd:YAG-pumped dye lasers with wavelength extension for frequency doubling and/or mixing after doubling. To achieve PLIF excitation for fuel and (1,0) band OH, Rhodamine 590 dye is used. The dye output is frequency doubled to produce excitation wavelengths near  $\lambda = 282$  nm, with  $1.0 \text{ cm}^{-1}$  bandwidth. The pulse width is 7 ns. Near these wavelengths, the pulse energy is typically maintained at 25 mJ – 30 mJ. The same wavelength is used to obtain the planar Mie scattering data. Fuel PLIF is achieved by tuning the dye laser to a wavelength that does not excite OH, but that does excite aromatic compounds in the fuel. The output from the laser is allowed to expand freely over the course of its path. These distances in the CE5 facility are approximately 15 m to the flame tube and 20 m to the sector. The path length in the ASCR facility is approximately 32 m. The laser beam is shaped into a laser sheet using an  $f = 3$  m (for CE5) or  $f = 2$  m (in ASCR) cylindrical lens, producing a sheet with dimensions roughly  $300 \mu\text{m}$  thick by 25 mm long.

A tunable KrF excimer laser was used for the UV-Raman experiment described in this paper. The laser used a “single-pass” configuration<sup>12</sup> producing approximately 90% linearly polarized light. The excimer laser output could be tuned from 247.8 nm to 248.8 nm, with typical pulse energies of 200 mJ in a pulse width of 13 ns. The laser was operated with a 3 Hz repetition rate. Upon exiting the laser, the beam was resized and collimated. Near the test section, a fused-silica spherical lens of focal length 250-mm was used to focus the beam into the center of the combustor flow path. The resultant beam’s cross section was approximately  $0.5 \text{ mm} \times 1 \text{ mm}$ . Although a lens having a longer focal length would have produced a narrower beam with a more uniform cross section throughout the test section, such a long focal length lens also generates energy densities sufficient to damage the input window.

Figure 6 shows a schematic drawing of the typical optical setup used for these experiments. The test cell coordinates are also shown, in which x, y and z are the horizontal, vertical, and axial components. The 2-D imaging and spectrometer cameras are on opposite sides of the test rig. As shown in the figure, the laser sheet (or beam) is inserted vertically, from top to bottom. The camera or spectrometer is set up to collect light scattered or emitted normal to the laser sheet. All images were obtained using gated, 16-bit, intensified CCD cameras having a  $384 \times 576$ -pixel array. The gate time was typically 75 ns. A remotely operated filter wheel was used to position the appropriate filter ahead of the lens, which was a Nikon 105-mm f/4.5 UV Nikkor camera lens. The filter used for Mie imaging was an interference filter centered at 283 nm, with a 2.6 nm full-width at half-maximum (FWHM) and transmission of 6%. The filter used for fuel and OH PLIF was an interference filter with a peak transmittance of 16% at a wavelength of 316 nm and FWHM of 1.6 nm. The interference filter used for  $\text{C}_2$  was centered at 514 nm and had a bandwidth of 10.8 nm FWHM. Its transmission was 40%.

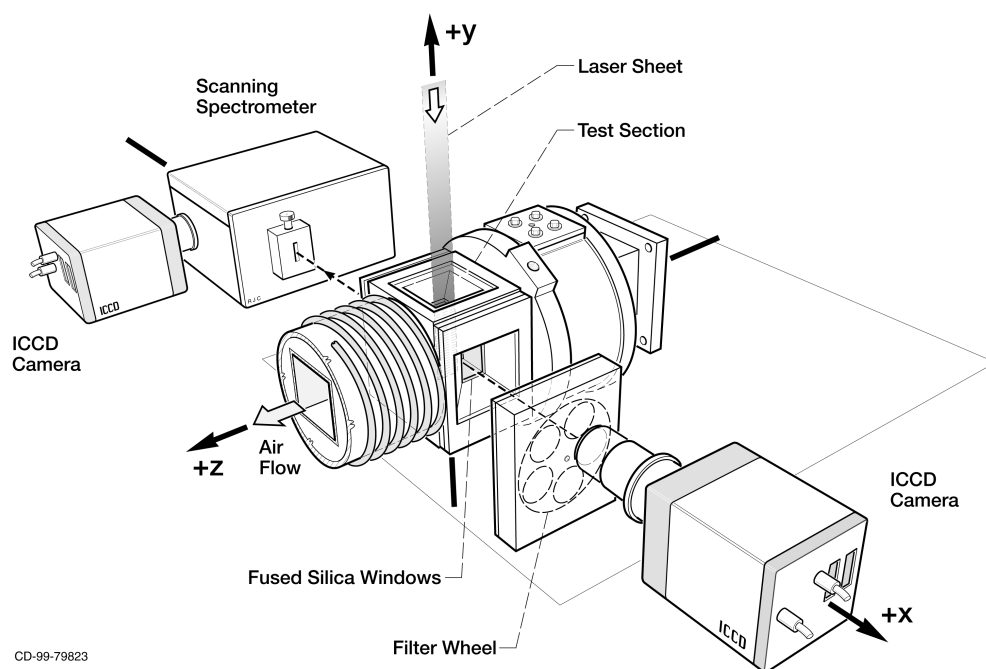


Figure 6 Drawing of the optical setup for combustion experiments

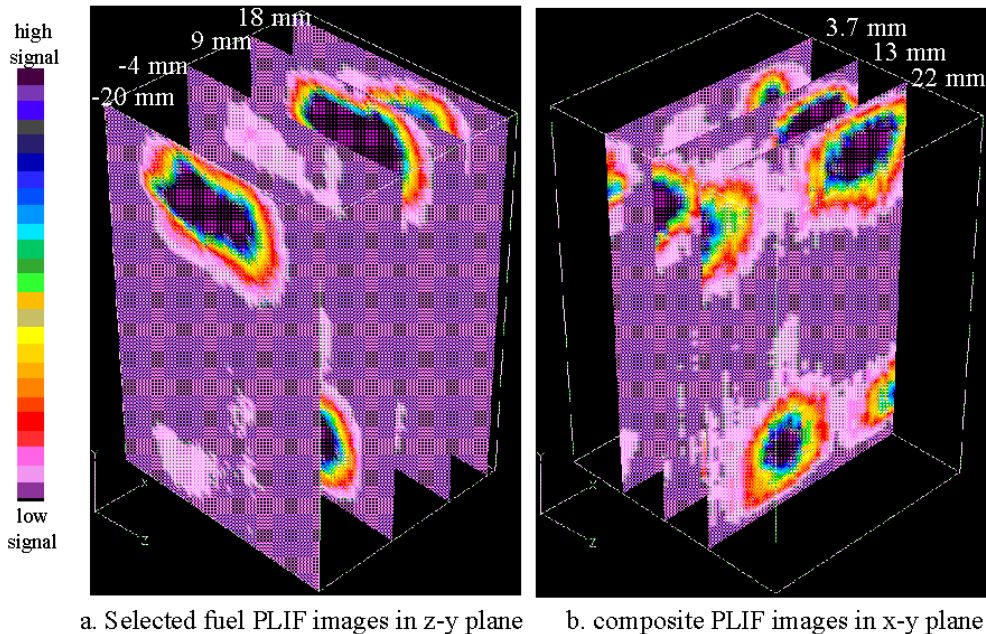


Figure 7 Example of 3-D image field generation. a. "Raw" z-y plane camera images (side views, parallel to direction of flow) are placed in a computational grid. b. Images projected in x-y planes (end views).

Some measurements are made by taking a spatial sequence (typically with 1-mm spacing) of two-dimensional planar laser-induced fluorescence (PLIF) or Mie scattering digital images. These images are taken in planes parallel to the flow axis,  $z$ . Movement of the laser sheet and the cameras is coordinated so that the distances between them remain fixed as the laser is scanned across the flow in the  $x$  direction. Placing them in a three-dimensional grid, as illustrated in figure 7a, the images are then processed. The resultant composite block can then be observed from any perspective. The results are typically presented as the original side view images and as the cross-sectional (end view) composite slices, as in figure 7b. The side view images are useful for fuel spray angle determination and to determine the (axial) progression of reaction species. End views allow one to assess fuel injector patterning and symmetry and the relative radial location of species. When appropriate, end views are used for fuel-air ratio imaging<sup>13</sup>.

Images are displayed using twenty-seven levels as depicted in the color bar shown on the left side of figure 7. The bar consists of twenty-five colors, plus black (low) and white (high). Each color accounts for approximately 10 counts (four percent) in the linear span from 0 counts to 255 counts of signal. Black represents the lowest two counts in signal; white represents the highest two signal values of 254 and 255.

## 4. SAMPLE RESULTS

### 4.1 CE5 sector rig—PLIF, PMie and emission spectra

Figures 8 and 9 show examples of data obtained from tests conducted using a single airblast injector having pilot and main fuel circuits. Only the outer region of the injector is optically accessible, due to the location of the windows above the centerline of the sector rig. For this test, the ceramic was cast to produce a circular flow path and the window surfaces were set back from rather than flush with the flow. End views of fuel PLIF, OH PLIF, and PMie imaging are shown for distances from the injector of 1.9 mm to 27.4 mm, as indicated by the numbers at the top of each column. The inlet conditions are  $T_{\text{inlet}} = 716 \text{ K}$ ,  $P_{\text{inlet}} = 17.7 \text{ atm}$  (high power) for figure 8 and  $T_{\text{inlet}} = 674 \text{ K}$ ,  $P_{\text{inlet}} = 8.4 \text{ atm}$  (low power) for figure 9. The equivalence ratio ( $\phi$ ) is 0.502 for both cases and the ratio of pilot to main fuel splits is the same. The laser sheet was scanned 46 mm across the flow. Each image was an on-chip average of 50 laser shots. The images are not corrected for laser sheet energy profile, which has a Gaussian ramp-up and falloff. Thus the fuel PLIF and PMie images near the fuel injector exit appear to have smaller concentration than some images considerably farther downstream. This probably also holds for OH PLIF signals farther downstream. Each species (row) is scaled based on the entire set of data taken. Therefore, one can compare the signals between these inlet conditions by species, and at each position as the point of view moves downstream.

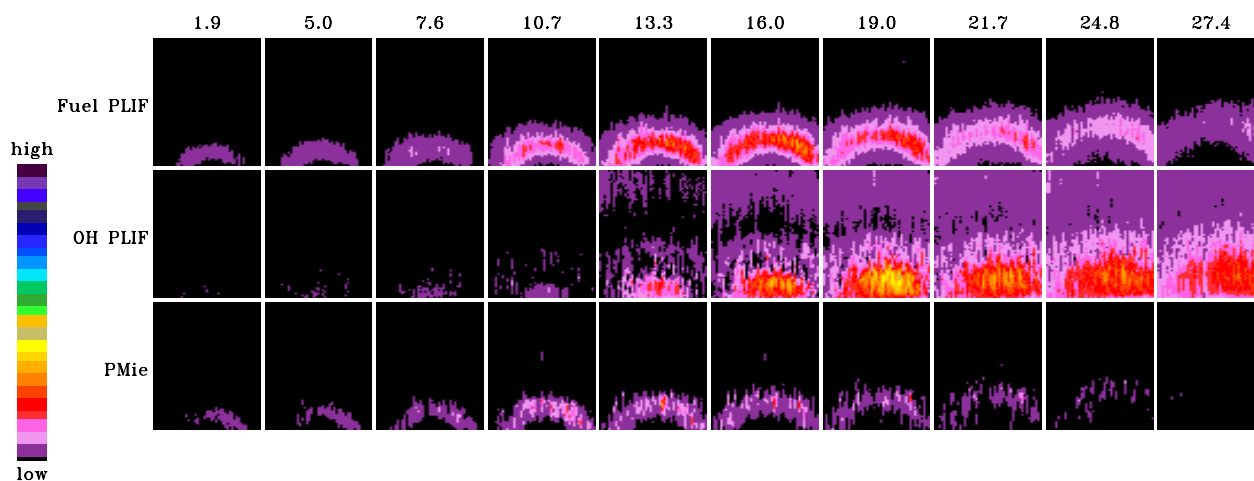


Figure 8 Fuel PLIF, OH PLIF, and PMie scattering end views for the CE5 sector high power test condition.  $T_{inlet} = 716K$ ,  $P = 17.7 \text{ atm}$ ,  $\phi = 0.502$ . Images are scaled with respect to species, for direct comparison to images of figure 9.

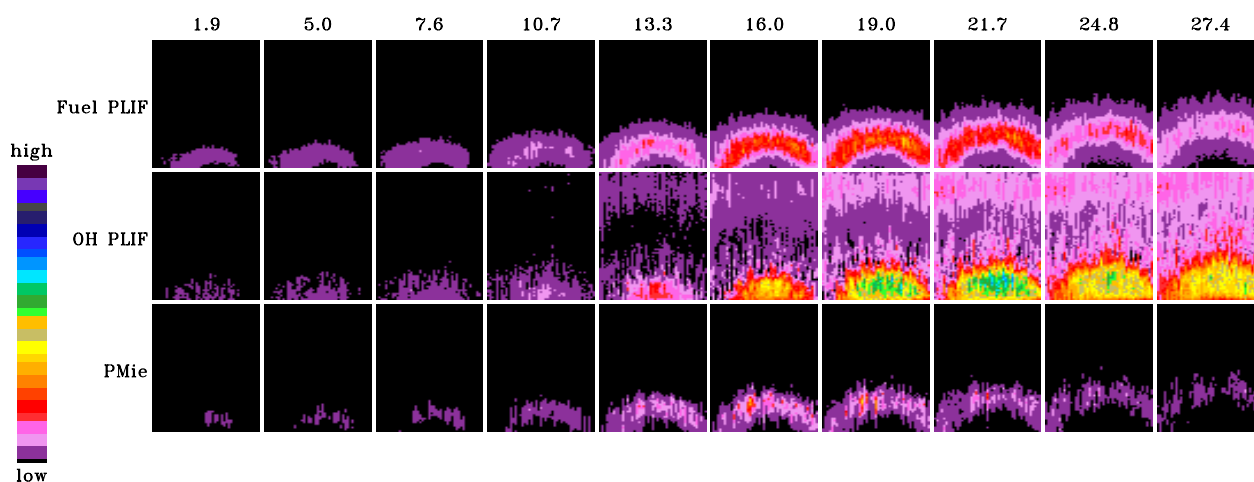


Figure 9 Fuel PLIF, OH PLIF, and PMie scattering end views for the CE5 sector low power test condition.  $T_{inlet} = 674K$ ,  $P = 8.4 \text{ atm}$ ,  $\phi = 0.502$ . Images are scaled with respect to species, for direct comparison to images of figure 8.

The PMie and fuel PLIF images show that the fuel/air mixture expands away from the injector as a hollow-cone spray. The OH PLIF images show that OH is formed primarily within the hollow cone of the spray and secondarily in the recirculation region outside of the spray—seen in the upper part of the OH images. The low power case (figure 9) shows that less of the fuel is vaporized as evidenced by the stronger Mie scattering signals seen in the figure. This is so even though the fuel flow rate entering the combustor is roughly 75% of the high power rate. Also observe that liquid travels farther into the combustion zone for the lower power case. There is also considerably more OH present as well as a stronger recirculation region. There is roughly twice as much OH produced for this condition than for the higher power case. In fact, of all conditions run, these two conditions represent the highest OH and the lowest OH produced. The much greater OH PLIF signal of the low power case compared to the high power case suggests a higher reactivity and heat release, therefore higher flame temperature for this case. As determined by the calculated results based on gas emissions sampling and the metered fuel and air flow rates, the low power condition produced higher flame temperatures and as many oxides of nitrogen as the high power condition.

Flame emission spectra were also taken during these tests (primarily to identify background noise and regions of relative spectral cleanliness for future applications). The 300 mm, f/4 spectrometer was set up as shown in figure 6. No lens was used to collect and focus light on the entrance slit, which was set at 100 microns. This was done so as not to saturate the camera, which was operated ungated with an exposure time of 0.1-s. These spectra were obtained using a 600 groove/mm holographic grating blazed at 300 nm. The spectral width using this grating-CCD array was approximately 60 nm. Individual spectra, each of 100 accumulations, were taken in the range from 180 nm to 900 nm and glued together; the minimum overlap was 10 nm.

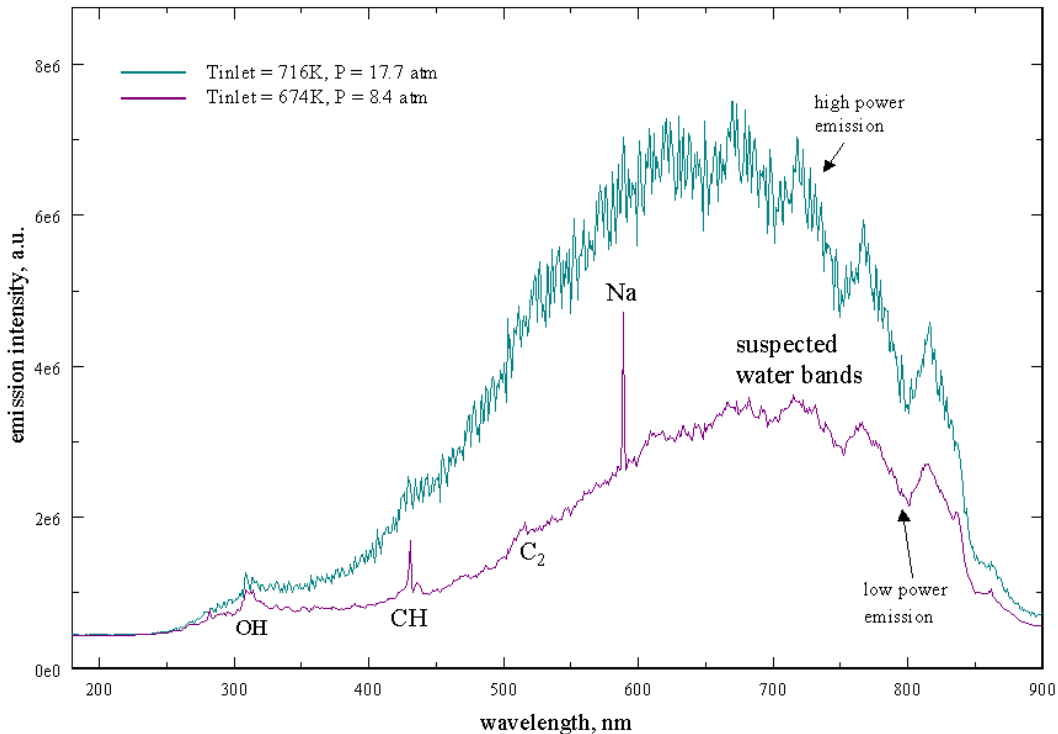


Figure 10 Emission spectra obtained for the high power (upper curve, in blue) and low power points during the CE5 sector test. Test conditions are as noted on the graph. The equivalence ratio is 0.5.

Figure 10 shows the spectra obtained for the two cases described above. One sees a continuum with fine atomic and broad molecular structure overlaid, including that of the radiant ceramic liner. The spectrum obtained from the high power case has over twice the area of the low power case, which is to be expected given the greater number of molecules available to emit light. In the low power case OH, CH, and the Swan C<sub>2</sub> bands may be clearly seen near 308 nm, 430 nm, and 516 nm. The high power spectrum is noisier and there may be some slight pressure broadening, but OH and CH can be seen with relatively little effort. There is a progression of bands in the visible and near infrared up through the usable range of the grating, roughly 850 nm. Each spectrum displays a sharp atomic peak at 589-nm, believed to be sodium. The peak is clearly dominant in the low power case. For the series of data taken, only those at this pressure condition (there were two others) had such a dominant peak. These conditions also correspond to the cases that had strong recirculation zones. Therefore, it is possible that small amounts of the castable liner, material, which uses sodium in the binding agent, are abraded from the liner surface and swept into the hot combusting region, and in turn emit this characteristic sodium line.

#### 4.2 CE5 Flame tube—spontaneous UV Raman scattering

The example from the flame tube rig demonstrates the first use of 1-D, UV, spontaneous Raman imaging in this type of combusting flow<sup>14</sup>, illustrated using figures 11 – 13. For this experiment, an injector based on the lean, premixed, pre-vaporized (LPP) concept was tested, in which the fuel is injected into a chamber that allows the fuel to evaporate and mix

with the incoming combustion air prior to delivery into the combustor. Nguyen<sup>15</sup> gives a general description of the injector. As described earlier, the  $\lambda = 248$  beam from the laser was collimated in the laser room. Just before entering the flame tube, the beam passed through an  $f = 250$  mm spherical lens, to produce a focused beam with a 0.5-mm by 1-mm cross section. The Raman-scattered light was collected through a side window using spherical lenses and refocused on the 100- $\mu\text{m}$  wide slit of the  $f = 250$  mm,  $f/4$  spectrograph. The combination of optics and spacing focused the central 6 mm of the beam through the 51-mm high flow path. A cuvette containing a dilute solution of butyl acetate was placed in front of the slit so as to reduce—but not eliminate—Rayleigh scattering<sup>14, 16</sup>.

The light was transmitted by the spectrograph to an intensified CCD camera. The camera's intensifier gate was set at 100 ns. Line spectra—such as those shown in figure 13—were acquired in one of two ways. In the first, 100 separate single-shot events were obtained. In the second, 100 events were accumulated on the detector array, providing a real-time, on-chip average. The image spectra shown in figures 11 and 12 were acquired via on-chip averaging. The observed Raman vibrational lines in wavenumbers ( $\text{cm}^{-1}$ ) are carbon dioxide 1388  $\text{cm}^{-1}$  and 1285  $\text{cm}^{-1}$ , oxygen at 1556  $\text{cm}^{-1}$ , nitrogen at 2331  $\text{cm}^{-1}$ , fuel (mainly C-H stretch) around 3050  $\text{cm}^{-1}$ , and water at 3657  $\text{cm}^{-1}$ . The abscissas of the spectra are wavelength, and the species locations are denoted.

Figure 11 shows an image obtained prior to combustion with heated air only flowing through the combustor. The image was obtained by summing the scattered light from 100 laser shots into the 550 K, 15 atm air. The vertical axis is the 6 mm height viewed within the combustor. From left to right in the figure are the butyl acetate-attenuated Rayleigh scattering of the 248 nm laser line and the vibrational Raman bands of oxygen and nitrogen. The asymmetry along the vertical axis is due to a slight optical misalignment. Eight such spectra were taken at different temperatures and pressures. The ratios of nitrogen to oxygen Raman intensities were within a  $\pm 2.3\%$  range, signaling good measurement precision.

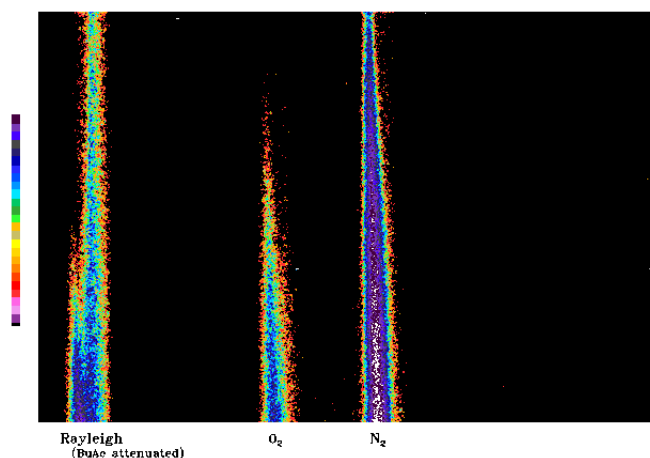


Figure 11 Air-only 1-D UV Raman image at 550K, 15 atm. The image was obtained by summing 100 laser shots.

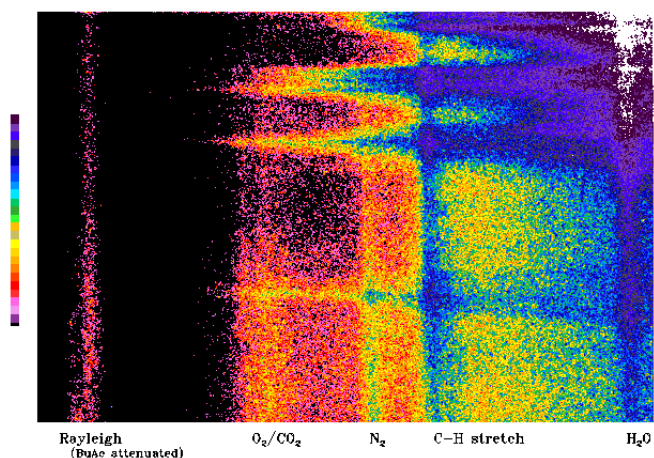


Figure 12 1-D UV Raman image during combustion at 10.8 atm and  $T_{\text{inlet}}$  of 755K. Species are identified along the horizontal axis. The  $\text{O}_2$  and  $\text{CO}_2$  lines are overlapped.

Figure 12 shows an image obtained with the combustor lit. It is the sum of 100 shots acquired at inlet temperature of 755K, rig pressure of 10 atm, combustion temperature of 1920K, and equivalence ratio of 0.514. From left to right are the (attenuated) Rayleigh, oxygen and carbon dioxide lines, nitrogen, C–H stretch, and water lines. The strongest lines are those from C–H stretch and water. Note that the  $\text{O}_2$  line is not cleanly separated from the two  $\text{CO}_2$  lines. This is a relatively minor disadvantage because the reactant and product species are determined primarily by following fuel and  $\text{H}_2\text{O}$  respectively, whereas the  $\text{O}_2$  and  $\text{CO}_2$  are directly related by stoichiometry.

The expanding horizontal streaks found at longer wavelengths in figure 12 are caused by intense fluorescence from PAH components of the fuel. These streaks are observed in only a few of the single-shot images. This indicates that in the summed 100-shot images, the relatively small number of single-shot images that contain them contributes these features.

Because there is no corresponding Mie scattering observed at this condition, these fluorescence streaks are not likely to emanate from fuel droplets. More likely, they may be indicative of local vapor clusters of newly evaporated fuel droplets. These streaks are more frequent in the upper half of the combustor flow images, coinciding with the observation of more fuel, and product water at this location. In addition to the horizontal streaks, also observed in this and all combustor conditions was an increasing amount of non-localized emission toward the right, also arising from the fluorescence from electronically excited PAH. Note that the extent of the non-localized emission along the abscissa is roughly the same as that of the horizontal streaks.

Figure 13 shows a comparison between a single shot spectrum (top) and a spectrum that is the sum of 100 shots in real-time. Aside from the single-shot spectrum being noisier, it displays all the features of the integrated sum and serves to demonstrate the sensitivity of the technique.

It was also observed that as the inlet temperature decreased, more liquid fuel passed through the measurement volume. In these instances—not shown here—Mie signal was dominant, overriding the Raleigh and any Raman signal.

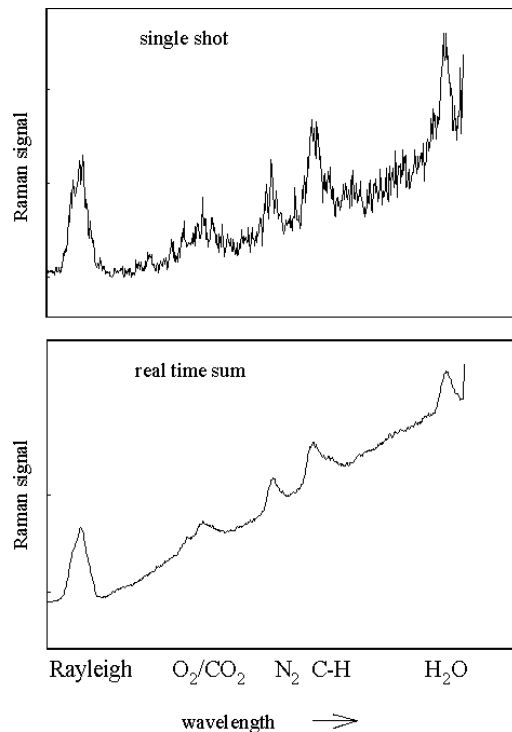


Figure 13 UV Raman flame spectra that compares single-shot (top) with on-chip average of 100 laser shots. The inlet temperature and rig pressure are 755K and 10.3 atm.

### 4.3 ASCR sector—PLIF, PMie, C<sub>2</sub> chemiluminescence

Tests were conducted on a double annular 15-degree combustor sector. The two fuel injectors, stacked one over the other, were of identical specification, with separate pilot and main fuel circuits. Figure 14 shows a photograph of the inner vessel's outer casing and windows. The 1.3 cm thick side windows had a clear aperture of 7 cm high by 5.7 cm long (axial direction). The side windows were positioned such that only flow from the top injector could be seen. The top windows of the combustor casing and liner were 0.64 cm thick. The smaller liner window measured 1.3 cm wide by 6.0 cm long. Once the top windows were installed, the combination of the window mounting hardware and compression of the sealing gasket material reduced the effective clear aperture of this top "slit" to about 3 mm wide by 5.7 cm long. The top windows were positioned over the injectors' central vertical plane.

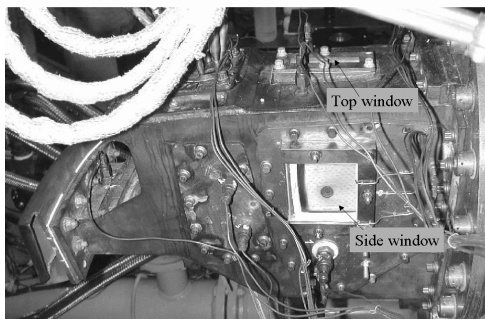


Figure 14 ASCR sector inner shell and windows. Flow is from left to right. At left is the flow conditioner/diffuser. Fuel injectors are mounted just upstream of the windows.

Table 1 Inlet conditions for the ASCR sector tests

Test point	P <sub>inlet</sub> , atm	T <sub>inlet</sub> , K	Fuel-air equivalence ratio, $\phi$
A	5.4	602	0.24
B	13.6	770	0.46
C	35	789	0.40
D	35	783	0.46
E	42	756	0.40
F	42	756	0.46

The laser was not traversed across the flow for these experiments because of the restrictive width of the top entrance windows. Traversing stages were used to accommodate for rig growth, 2.5 cm to 3.0 cm for this particular test series. Because the camera was positioned farther from the flow due to the large outer shell radius, the field of view was smaller than is typical of the CE5 facility. As a result, a 384 by 330 subset of the detector's array was used.

OH and fuel PLIF, planar Mie scattering of liquid fuel, and  $C_2$  chemiluminescence data were taken for the six points listed in table 1. For each inlet condition, 100 single shot frames were obtained. The time between "snapshots" is approximately 0.4-s; therefore, each file required roughly 40-s to 50-s to acquire. In addition, on-chip-averages were acquired of 100, 200, or 300 laser shots. In the case of  $C_2$ , emissions derive from chemiluminescence induced by the combustion process; thus the laser was not allowed to pass through the combustor at those times. All images—including the  $C_2$  emissions—were acquired with a 75-ns gate. Although PMie images were acquired, none are shown here because, with the exception of the lowest power condition, there was little or no Mie signal, signifying that the fuel was nearly 100% vaporized.

Figure 15 shows ten consecutive single-shot images of  $C_2$  emissions in the flame at test point F with a 0.46 equivalence ratio. These single-shot images show the shot-to-shot variation in the flow. Although each frame is different, the overall "structure" of the species field is the same and the single-shot structure is not very different from that observed in the average of 100 frames, shown at the bottom right in figure 16.

Figure 16 shows a side-by-side comparison of the fuel PLIF (left) and OH PLIF data in the first two columns and  $C_2$  chemiluminescence averages (right) for the six test points. Each image is the average of 100 single-shot images. Each row represents a different inlet condition. Engine power increases from top to bottom. The first row is test point A. The second row is test point B. The third and fourth rows show data at points C and D, for which the inlet temperature is nominally the same, but the equivalence ratio is varied. The fifth and sixth rows are test points E and F, which also are different only in equivalence ratio. Images within species are presented on the same scale to show the relative changes in signal from point to point. Each species is scaled separately. One difference between point A and the other test points is that a little more fuel is present near the projected centerline of the injector (which runs across the center of the images). This case reflects the fact that the pilot fuel circuit is the only one fueled at this point. The  $C_2$  emissions are clearly different at this condition than for all other engine conditions. Another difference for test point A is the location of the fuel jet. The fuel PLIF images show that the pilot fuel jet lies closer to the injector centerline. For the other flow conditions, the fuel jet lies parallel to the pilot spray but farther from the centerline. OH is in roughly the same location for all conditions, slightly downstream of the fuel PLIF signal, on the fuel-lean regions of the fuel spray. Thus for point A, OH is below the fuel and for all other engine conditions, above the fuel spray. The  $C_2$  emissions are found to be highest at this inlet condition.

The PLIF signals are the highest at point B. The key difference between conditions C and D is the fuel-air ratio. The same is true of cases E and F, at 42 atm. In each case, the higher signal corresponds to the higher fuel-air ratio. For the PLIF data, the highest-pressure conditions have slightly lower signal. This is likely to be an effect of quenching of the fluorescence signal at higher pressures. Further analysis is necessary to determine the reasons for the differences in signal strength.

Very little of any measured species is present above the top injector's centerline (top half of the images). Since the injector is symmetric, one would expect to see above the centerline a "jet" of fuel similar to the one below the centerline. One possible explanation for this is that the fuel injector had a plugged main fuel circuit. Another possibility is that the species below the centerline are seen primarily due to the effect of its interaction with the main fuel circuit of the bottom injector. A hint of the effluent from the bottom injector can sometimes be seen at the bottom of some of the OH PLIF and  $C_2$  images. For OH, these are most easily seen at test points A, B, and F. For  $C_2$ , signal that emanates from the bottom injector can be seen at the bottom of images for all conditions except point D. The inability to traverse across the flow due to the limitation imposed by the small top window prevents a direct determination of whether the asymmetry is real. However, the  $C_2$  luminosity (which has similar trends as the PLIF data) is not restricted in space by the thin laser sheet but instead comes from all points within our field of view of the flow. The implication then is that the asymmetry is indeed real. The ratio of strength of signal for  $C_2$  below the centerline compared to above the centerline is at least 2.5-to 1.

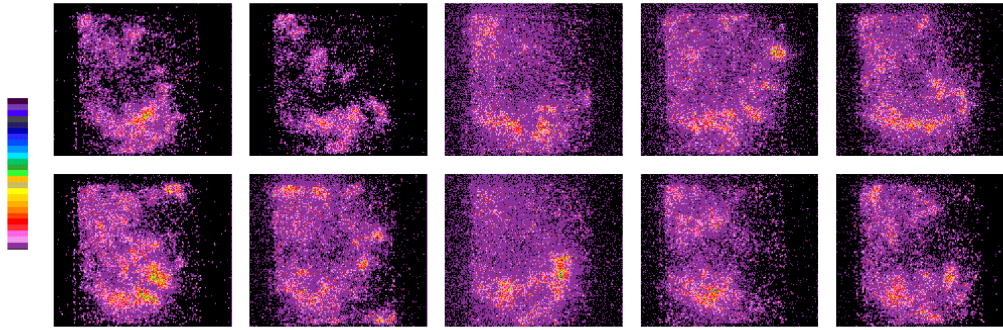


Figure 15 Ten consecutive single "snapshots" of flame  $C_2$  emission in the ASCR combustor sector at  $T_{inlet} = 756K$ ,  $P = 42$  atm, and 0.46 equivalence ratio. Each image was acquired in 75-ns.

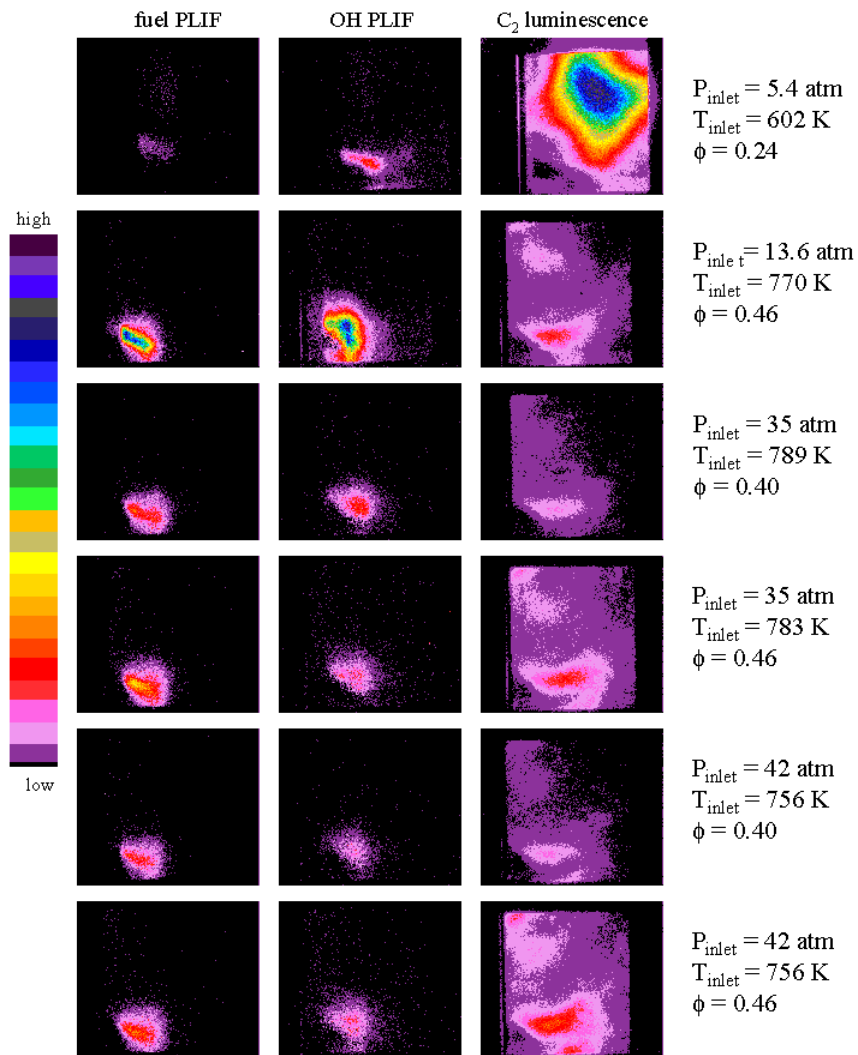


Figure 16 Comparison of fuel PLIF, OH PLIF, and  $C_2$  chemiluminescence for the conditions shown at the right of each row. Images are scaled per species (column).

## 5. SUMMARY

Using emissions spectra and visualization techniques, fuel injection, fuel/air mixing, and some reaction zone species were measured *in situ* within realistic combustor flame tubes and sectors in order to characterize combustor and fuel injector performance. The combustor facilities are designed to supply the flow rates, inlet temperatures and pressures anticipated for future, high-efficiency engines. These combustors use concept fuel injector hardware that might be used in future high temperature, high pressure, and low emissions combustors. The data are used to diagnose the performance of injectors and to design new fuel injectors with overall engine performance goals of increased efficiency and reduced environmental impact. Fuel injector spray patterns are measured using fuel PLIF images, obtained in the region for OH (1,0) band excitation. Mie scattering is used to image the liquid fuel that enters the combustor. OH PLIF has been useful in marking flame and recirculation zones and also has indicated hot zones. In addition to visualizing the location of these combustion species relative to the fuel injector, the results demonstrate the decay of fuel concentration and the concomitant increase in OH as the reaction proceeds. These trends are data used by combustor and fuel injector designers and by kinetics modelers. The data provide a database for initial and boundary conditions for model validation. Engine designers have modified their injector designs based on the novel data obtained using the aforementioned visualization techniques. 1-D, UV Raman imaging was applied and demonstrated to be a viable technique for this type of combustion environment despite the associated LIF interferences from PAH and Mie scattering from drops at low inlet temperatures.

## 7. REFERENCES

1. C. Löfström, H. Kaaling, and M. Aldén, "Visualization of fuel distributions in premixed ducts in a low-emission gas turbine combustor using laser techniques," *Twenty-Sixth Symp. (Int'l) on Combustion*, pp. 2787–2793, 1996.
2. Y.R. Hicks, R.J. Locke, R.C. Anderson, M. Zaller, and H.J. Schock, "Imaging fluorescent combustion species in gas turbine flame tubes: on complexities in real systems," Paper AIAA 97-2837, 1997.
3. D.A. Greenhalgh, "Planar measurements of fuel vapour, liquid fuel, liquid droplet size and soot," RTO lecture series 217, RTO-EN-6, reference 7, 1999.
4. P. Andresen, G. Meijer, H. Voges, A. Koch, W. Hentschel, W. Oppermann, and E. Rothe, "Fluorescence imaging inside an internal combustion engine using tunable excimer lasers," *Appl. Optics*, **29**, pp. 2392–2404, 1990.
5. M. Versluis, M. Boogaarts, R. Klein-Douwel, J.J. ter Meulen, W.L. Meerts, and G. Meijer, "Laser-induced fluorescence imaging in a 100-kW natural gas flame," *Applied Physics B*, **55**, pp. 164–170, 1992.
6. R.J. Locke, Y.R. Hicks, R.C. Anderson, and M.M. Zaller, "Optical fuel Injector patterning measurements in advanced liquid-fueled, high pressure, gas turbine combustors," *Combustion Science and Technology*, **138**, pp. 297–311, 1998.
7. D.F. Marran, M.B. Long, W.M. Studzinski, J.C. Swindal, and W.P. Acker, "Planar laser-induced fluorescence imaging of crevice hydrocarbon emissions in a spark-ignited engine," *Twenty-Seventh Symp. (Int'l) on Combustion*, pp. 2069–2076, 1998.
8. Y. Deguchi, H. Nakagawa, T. Ichinose, and M. Inada, "LIF applications for practical combustors," *Journal of Visualization*, **2**, pp. 343–351, 2000.
9. Y.R. Hicks, R.J. Locke, M.M. Zaller, R.C. Anderson, and K.A. Ockunzzi, "Combining planar Mie scattering and fluorescence imaging techniques to analyze fuel injection and combustion performance in aviation gas turbine combustors," Proceedings of VSJ-SPIE98, AB081, Yokohama, 1998.
10. J.C. Brooda, S.S. Seo, R.J. Santoro, G. Shirhattikar, and V. Yang, "An experimental study of combustion dynamics of a premixed swirl injector," *Twenty-Seventh Symp. (Int'l) on Combustion*, pp. 1849–1856, 1998.
11. N. Kawahara, Y. Ikeda, and T. Nakajima, "Measurements of the combustion characteristics of compound clusters in pressure-atomized spray flame," Paper AIAA 99-0210, 1999.
12. G. Grünefeld, P. Andresen, H. Schlüter, and E.W. Rothe, "Operation of a tunable excimer laser with KrF and ArF without Cassegrain optics," *Appl. Phys.*, **B62**, pp.241–247, 1996.
13. R.J. Locke, M. Zaller, Y.R. Hicks, and R.C. Anderson, "Non-intrusive laser-induced imaging for speciation and patterning in high pressure gas turbine combustors," in *Optical Diagnostics for Fluids/Heat/Combustion/and Photomechanics for Solids*, S. Cha, P.J. Bryanston-Cross, and C.R. Mercer, Editors, Proc. SPIE 3783, pp. 332–338, 1999.
14. Y. Gu, E.W. Rothe, G.P. Reck, R.C. Anderson, Y.R. Hicks, M. Zaller, Q.-V. Nguyen, and R.J. Locke, "Raman imaging from a high-pressure, jet-a fueled gas turbine combustor," paper AIAA-2000-0073, 2000.
15. Q.-V. Nguyen, R.K. Mongia, and R.W. Dibble, "Real-time optical fuel-to-air ratio sensor for gas turbine combustors," NASA Technical Memorandum NASA/TM—1999-20941, 1999.
16. P.J. Hargis, "Trace detection of N<sub>2</sub> by KrF-laser excited spontaneous Raman Spectroscopy," *Appl. Optics*, **20**, pp. 149–152, 1981.

# REPORT DOCUMENTATION PAGE

*Form Approved*  
*OMB No. 0704-0188*

Public reporting burden for this collection of information is estimated to average 1 hour per response, including the time for reviewing instructions, searching existing data sources, gathering and maintaining the data needed, and completing and reviewing the collection of information. Send comments regarding this burden estimate or any other aspect of this collection of information, including suggestions for reducing this burden, to Washington Headquarters Services, Directorate for Information Operations and Reports, 1215 Jefferson Davis Highway, Suite 1204, Arlington, VA 22202-4302, and to the Office of Management and Budget, Paperwork Reduction Project (0704-0188), Washington, DC 20503.

<b>1. AGENCY USE ONLY</b> ( <i>Leave blank</i> )	<b>2. REPORT DATE</b> September 2000	<b>3. REPORT TYPE AND DATES COVERED</b> Technical Memorandum	
<b>4. TITLE AND SUBTITLE</b> Optical Measurement and Visualization in High-Pressure, High-Temperature, Aviation Gas Turbine Combustors		<b>5. FUNDING NUMBERS</b>  WU-714-02-40-00	
<b>6. AUTHOR(S)</b>  Yolanda R. Hicks, Randy J. Locke, and Robert C. Anderson			
<b>7. PERFORMING ORGANIZATION NAME(S) AND ADDRESS(ES)</b> National Aeronautics and Space Administration John H. Glenn Research Center at Lewis Field Cleveland, Ohio 44135-3191		<b>8. PERFORMING ORGANIZATION REPORT NUMBER</b>  E-12431	
<b>9. SPONSORING/MONITORING AGENCY NAME(S) AND ADDRESS(ES)</b> National Aeronautics and Space Administration Washington, DC 20546-0001		<b>10. SPONSORING/MONITORING AGENCY REPORT NUMBER</b>  NASA TM-2000-210377	
<b>11. SUPPLEMENTARY NOTES</b> Prepared for the EOS/SPIE Symposium on Applied Photonics cosponsored by the European Optical Society and the International Society for Optical Engineering, Glasgow, Scotland, May 22-25, 2000. Yolanda R. Hicks and Robert C. Anderson, NASA Glenn Research Center; and Randy J. Locke, Dynacs Engineering Company, Inc., 2001 Aerospace Parkway, Brook Park, Ohio 44142. Responsible person, Yolanda R. Hicks, organization code 5830, (216) 433-3410.			
<b>12a. DISTRIBUTION/AVAILABILITY STATEMENT</b>  Unclassified - Unlimited Subject Categories: 07, 09, 35 and 74  This publication is available from the NASA Center for AeroSpace Information, (301) 621-0390.		<b>12b. DISTRIBUTION CODE</b>	
<b>13. ABSTRACT</b> ( <i>Maximum 200 words</i> )  Planar laser-induced fluorescence (PLIF), planar Mie scattering (PMie), and linear (1-D) spontaneous Raman scattering are applied to flame tube and sector combustors that burn Jet-A fuel at a range of inlet temperatures and pressures that simulate conditions expected in future high-performance civilian gas turbine engines. Chemiluminescence arising from C <sub>2</sub> in the flame was also imaged. Flame spectral emissions measurements were obtained using a scanning spectrometer. Several different advanced concept fuel injectors were examined. First-ever PLIF and chemiluminescence data are presented from the 60-atm gas turbine combustor facility.			
<b>14. SUBJECT TERMS</b>  Planar laser-induced fluorescence; Mie imaging; Linear Raman scattering; Gas turbine combustors; Fuel injection; Combustion species imaging; Fluorescence; LIF; Mie scattering; Laser diagnostics		<b>15. NUMBER OF PAGES</b> 18	
		<b>16. PRICE CODE</b> A03	
<b>17. SECURITY CLASSIFICATION OF REPORT</b> Unclassified	<b>18. SECURITY CLASSIFICATION OF THIS PAGE</b> Unclassified	<b>19. SECURITY CLASSIFICATION OF ABSTRACT</b> Unclassified	<b>20. LIMITATION OF ABSTRACT</b>